



HI in High Gas-phase Metallicity Dwarf Galaxy WISEA J230615.06 +143927.9

Yan Guo^{1,2} , C. Sengupta¹ , T. C. Scott³ , P. Lagos³ , and Y. Luo¹

¹ Purple Mountain Observatory, Chinese Academy of Sciences, Nanjing 210023, China; sengupta.chandreyee@gmail.com

² School of Astronomy and Space Sciences, University of Science and Technology of China, Hefei 230026, China

³ Institute of Astrophysics and Space Sciences (IA Porto), Rua das Estrelas, 4150-762, Porto, Portugal

Received 2023 September 10; revised 2023 November 8; accepted 2023 November 21; published 2024 January 15

Abstract

We present resolved Giant Metrewave Radio Telescope HI observations of the high gas-phase metallicity dwarf galaxy WISEA J230615.06+143927.9 ($z = 0.005$) (hereafter J2306) and investigate whether it could be a Tidal Dwarf Galaxy (TDG) candidate. TDGs are observed to have higher metallicities than normal dwarfs. J2306 has an unusual combination of a blue $g - r$ color of 0.23 mag, irregular optical morphology and high-metallicity ($12 + \log(\text{O}/\text{H}) = 8.68 \pm 0.14$), making it an interesting galaxy to study in more detail. We find J2306 to be an HI rich galaxy with a large extended, unperturbed rotating HI disk. Using our HI data we estimated its dynamical mass and found the galaxy to be dark matter (DM) dominated within its HI radius. The quantity of DM, inferred from its dynamical mass, appears to rule out J2306 as an evolved TDG. A wide area environment search reveals J2306 to be isolated from any larger galaxies which could have been the source of its high gas metallicity. Additionally, the HI morphology and kinematics of the galaxy show no indication of a recent merger to explain the high-metallicity. Further detailed optical spectroscopic observations of J2306 might provide an answer to how a seemingly ordinary irregular dwarf galaxy achieved such a high level of metal enrichment.

Key words: galaxies: abundances – galaxies: dwarf – galaxies: irregular – radio lines: galaxies – radio lines: ISM

1. Introduction

Extrapolating from the local universe, low-mass dwarf galaxies are understood to be the most ubiquitous galaxies in the universe (Dale et al. 2009; McConnachie 2012), however, the local dwarfs remain relatively unexplored, because of the difficulty of observing such optically faint objects. It is in this regime where cosmological predictions differ most from observations and the large scatter in the observed values of dwarf properties makes it difficult to discern the underlying trends in their properties. Typically, dwarfs are dark matter (DM) dominated, faint irregular optical objects (e.g., Lagos et al. 2007), with their observed DM potentials being shallower than predicted by cosmological models (e.g., Oh et al. 2015). Dwarf galaxies are also observed to have significantly sub-solar metallicities, $12 + \log(\text{O}/\text{H}) = 7.4\text{--}7.9$, occasionally reaching extremely low values (Lee et al. 2003; Lagos et al. 2018, and references therein). Tremonti et al. (2004) using Sloan Digital Sky Survey (SDSS) DR4 data, demonstrated the strong positive correlation between galaxy stellar mass and metallicity ($12 + \log(\text{O}/\text{H})$). The scatter in the relation is much larger in the dwarf mass range and Peebles et al. (2008), applying restrictive selection criteria to the Tremonti et al. (2004) sample, identified 41 dwarf galaxies having metallicities between $8.6 \leq 12 + \log(\text{O}/\text{H}) \leq 9.3$, challenging the idea that dwarf galaxies are necessarily low-metallicity galaxies. Since the dwarf galaxy

population is dominated by low-metallicity objects, the rarely found high-metallicity dwarfs are particularly interesting. While a handful of such high-metallicity dwarfs have been detected, their formation scenarios or physical properties are yet to be explored in detail. One possible formation scenario for such high-metallicity dwarfs is formation out of metal-rich gas debris ejected during a tidal interaction between larger galaxies, at least one of which is gas rich (Duc & Mirabel 1999). These tidal dwarf galaxies (TDGs) are usually observed to have higher metallicities than normal dwarfs of the same stellar mass, see blue points in Figure 1 and (e.g., Duc & Mirabel 1999, Duc 2012; Smith et al. 2010; Scott et al. 2018). Other possible formation scenarios may include accretion of tiny evolved early-type dwarf galaxies. In this paper, we present Giant Metrewave Radio Telescope (GMRT) HI 21 cm imaging of the high-metallicity dwarf galaxy, SDSS J230614.96+143926.7 also known as WISEA J230615.06 +143927.9 (23^h06^m15^s.050 +14^d39^m27^s.50), hereafter referred to as J2306, selected from the SDSS. The previous single dish HI detection of the galaxy was with the Arecibo telescope (Haynes et al. 2011, AGC 332 413). Being nearby and having a prior single dish HI detection made J2306 a suitable candidate for a high-resolution HI study. More information on the galaxy's properties is provided in Section 2.1. Our aim is to

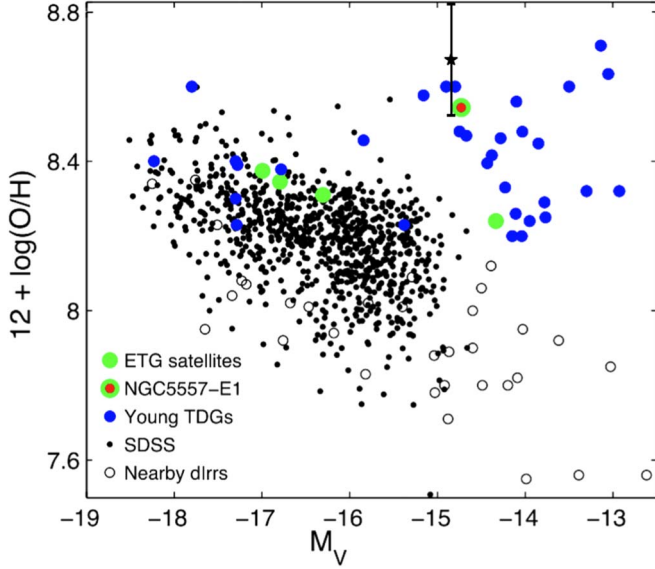


Figure 1. $12 + \log(\text{O}/\text{H})$ abundances from selected samples of dwarf galaxies plotted against their V -band magnitude (M_V) (Duc et al. 2014). The open circles are nearby dwarf irregulars from (Richer & McCall 1995; van Zee & Haynes 2006), the filled black dots represent normal SDSS dwarfs and the green filled circles and NGC 5557-E1 are early-type galaxy satellites from Duc et al. (2014), the filled blue circles are TDGs from Weilbacher et al. (2003), Boquien et al. (2010). See Figure 4 of Duc et al. (2014) for more detail. J2306 is plotted with a black star to show its properties relative to other dwarf galaxies.

increase the understanding of J2306’s physical properties and investigate possible formation scenarios.

Using the heliocentric optical velocity (1542 km s^{-1}) of J2306 from NASA Extragalactic Database (NED) and assuming $H_0 = 68 \text{ km s}^{-1} \text{ Mpc}^{-1}$ (Planck Collaboration et al. 2020), we adopt a distance of 22.7 Mpc to the galaxy. At this distance, the spatial scale is $\sim 6.4 \text{ kpc arcmin}^{-1}$. All α and δ positions referred to throughout this paper as J2000.

2. Data and Observations

2.1. The Source Properties and Metallicity Estimates

J2306 is a small nearby dwarf galaxy with an SDSS g -band absolute magnitude $= -14.83 \text{ mag}$, $g - r$ color $\sim 0.23 \text{ mag}$ and its r -band D_{25} diameter estimated from NED is $\sim 2.9 \text{ kpc}$. The galaxy is not an early-type dwarf, as its optical morphology is non-compact and irregular. Figure 2 shows the SDSS optical image of J2306. We used the relationship between photometric SDSS model magnitudes for selected color band filters and stellar M/L ratio from Bell et al. (2003), to estimate the galaxy’s stellar mass. The SDSS g -band luminosity (L_g) and $g - r$ color of the source were used to calculate stellar mass

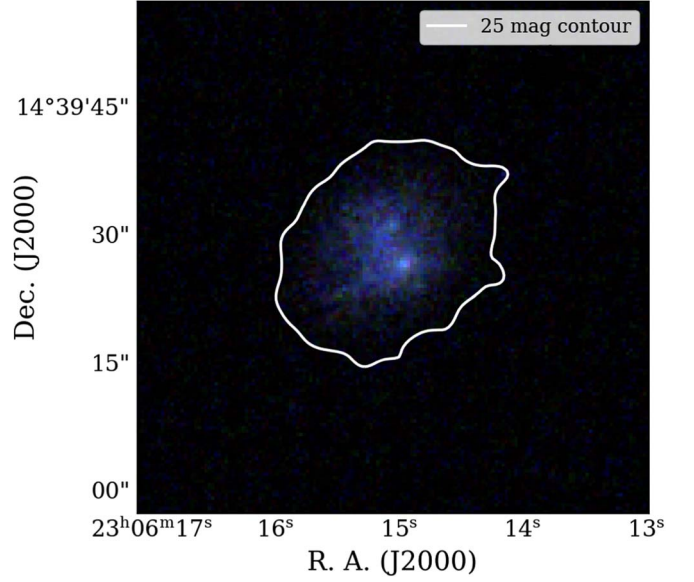


Figure 2. SDSS g , r , i band composite image of J2306, with the 25th magnitude shown with a white contour.

using Equation (1):

$$\log(M/L_g) = -0.499 + 1.519(g - r) \quad (1)$$

The stellar mass (M_*) of J2306, calculated using Equation (1) is $2.4 \times 10^7 M_\odot$, confirming it as a low stellar mass dwarf. Typically, the distance to a galaxy can be estimated from its recessional velocity which is related to the expansion rate of the universe via the Hubble constant. However, for galaxies with recessional velocities $< 1500 \text{ km s}^{-1}$ peculiar motions along the line of sight due to local gravitational forces can add significant additional uncertainty to the distance estimates. For J2306 adding or subtracting a typical group velocity dispersion (250 km s^{-1}) to the measured recessional heliocentric velocity (1542 km s^{-1}) changes the distance to the galaxy between 19.10 and 26.45 Mpc , which in turn implies $M_* = 1.7 \times 10^7 M_\odot$ and $3.2 \times 10^7 M_\odot$, respectively. This shows that, unless J2306 has an extraordinarily high peculiar velocity, it is a low stellar mass dwarf with M_* of the order $10^7 M_\odot$. J2306 is a faint galaxy that has an “unreliable photometry” flag in the SDSS database. As a result of the uncertainties in both distance and photometry for J2306, we treat our stellar mass calculation as only an order of magnitude estimate.

From J2306’s SDSS spectrum (Figure 3), we estimated its gas phase metallicity. The spectrum’s [O III] $\lambda 4363$ auroral emission line is weak and [O II] $\lambda 3727$ is beyond the SDSS spectrometer’s wavelength range, so the T_e method could not be used to calculate gas metallicity. Instead, we used the relation between metallicity and two strong line calibrators (N2 and O3N2) as prescribed in Denicoló et al. (2002), Pettini & Pagel (2004), Nagao et al. (2006), Pérez-Montero & Contini (2009),

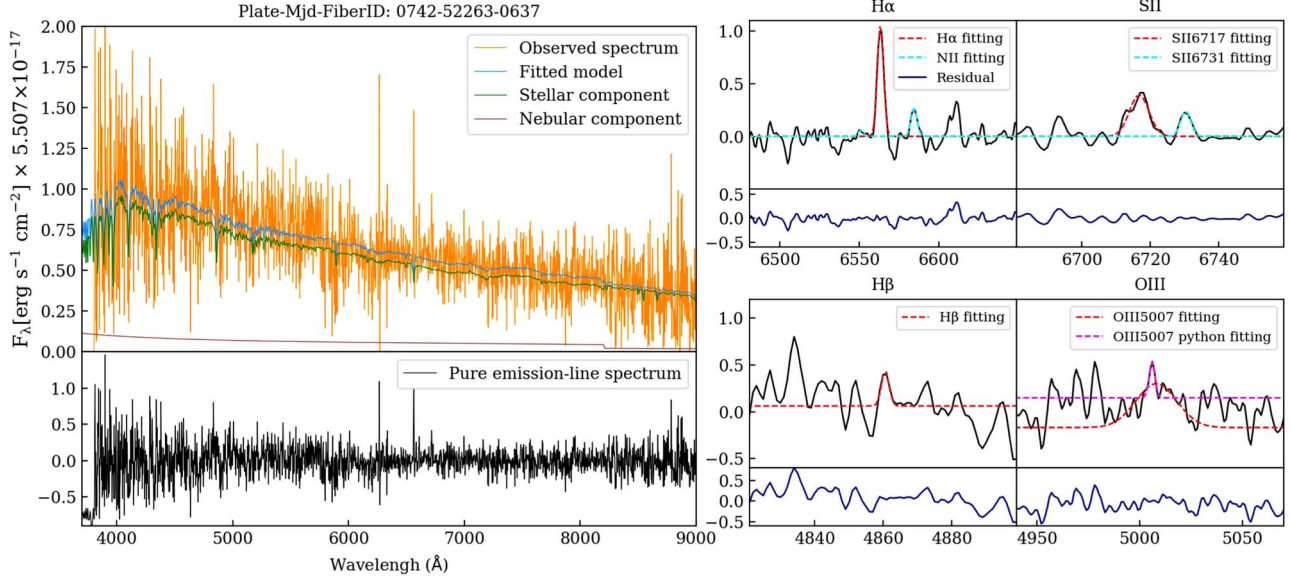


Figure 3. The top left panel shows the SDSS spectrum of J2306 along with FADO fits. The bottom left panel shows the pure emission-line spectrum. The four panels to the right shows the FADO fits to individual lines and their residuals. Line names are shown on top of each panel. The [O III] box has two different fits to the [O III] $\lambda 5007$ line. Due to poor SNR, the FADO fit (in red broken line) had failed. The line was then fitted using our own python code (shown in pink broken line). The [O III] $\lambda 4959$ line is unresolved.

Marino et al. (2013), Bian et al. (2018) and Curti et al. (2020) to estimate the $12 + \log(\text{O}/\text{H})$. We took the average value of the $12 + \log(\text{O}/\text{H})$ derived from the N2 and O3N2 calibrations by each of the above sets of authors to calculate the final gas metallicity value of J2306. The complete list of the $12 + \log(\text{O}/\text{H})$ calibrators from the selected authors used to calculate the galaxy's metallicity is given in Table 1.

The metallicity sensitive emission line ratios used in this work are the following:

$$\text{N2} = \log \left(\frac{H\alpha}{[\text{N II}] \lambda 6584} \right)$$

$$\text{O3N2} = \log \left(\frac{[\text{O III}] \lambda 5007}{H\beta} \times \frac{H\alpha}{[\text{N II}] \lambda 6584} \right)$$

Here $H\alpha$, $H\beta$, $[\text{N II}] \lambda 6584$, $[\text{O III}] \lambda 5007$ represent the extinction corrected intrinsic fluxes of the respective spectral lines. These metallicity indicators can be used for both, metal-poor and metal-rich galaxies in the range $7.31 < 12 + \log(\text{O}/\text{H}) < 8.84$ for the N2 and $7.82 < 12 + \log(\text{O}/\text{H}) < 8.78$ for the O3N2 emission line ratios on average. However, O3N2-based metallicity can reach values of $12 + \log(\text{O}/\text{H}) \leq 9.2$ (Nagao et al. 2006).

The population spectral synthesis (PSS) code FADO (Fitting Analysis using Differential evolution Optimization, Gomes & Papaderos 2017) was applied to the J2306 SDSS spectrum corrected for Galactic extinction based on Schlegel et al. (1998) color excess $E(B - V)$ map and the Cardelli et al. (1989) extinction law (CCM). The observed emission line fluxes of J2306 were obtained from FADO. We note that due to poor

Table 1
Metallicity for J2306 Using N2 Calibrators from Selected Authors

Calibrator	Reference	$12 + \log(\text{O}/\text{H})$
N2	Bian 2018	8.69 ± 0.20
N2	Curti 2020	8.72 ± 0.28
N2	Denicoló 2002	8.79 ± 0.23
N2	Marino 2013	8.53 ± 0.15
N2	Nagao 2006	9.01 ± 0.33
N2	Pérez-Montero 2009	8.71 ± 0.25
N2	Pettini 2004	8.68 ± 0.74
mean N2		8.73
std N2		0.13
O3N2	Bian2018	8.80 ± 0.45
O3N2	Curti2020	8.64 ± 0.26
O3N2	Marino2013	8.42 ± 0.20
O3N2	Pérez-Montero2009	8.58 ± 0.30
O3N2	Pettini2004	8.56 ± 0.31
mean O3N2		8.60
std O3N2		0.12
mean N2+O3N2		8.68
std N2+O3N2		0.14

SNR (see Figure 3) the FADO fit to the [O III] $\lambda 5007$ line failed. However that line was then re-fitted using our own python line fitting code and the flux obtained was utilized to calculate $12 + \log(\text{O}/\text{H})$ for J2306. The [O III] $\lambda 4959$ emission line is unresolved. We then corrected the intrinsic extinction for observed flux $F(\lambda)$ to determine the intrinsic emission-line

Table 2Observed $F(\text{H}\beta)$ in Units of $10^{-17} \text{ erg s}^{-1} \text{ cm}^{-2}$, de-reddened SDSS Emission Line Fluxes, Extinction $c(\text{H}\beta)$ and Emission Line Ratios

	$F(\lambda)/F(\text{H}\beta)$	$I(\lambda)/I(\text{H}\beta)$
$\text{H}\beta$	1.00 ± 2.96	1.00 ± 2.95
$[\text{O III}]\lambda 4959$
$[\text{O III}]\lambda 5007$	1.29 ± 2.69	1.18 ± 2.48
$\text{H}\alpha$	5.76 ± 12.13	2.86 ± 8.00
$[\text{N II}]\lambda 6584$	2.05 ± 4.51	1.01 ± 2.91
$[\text{S II}]\lambda 6717$	2.93 ± 6.32	1.39 ± 4.05
$[\text{S II}]\lambda 6731$	0.97 ± 2.16	0.46 ± 1.36
$F(\text{H}\beta)$	5.75 ± 0.46	
$c(\text{H}\beta)$	1.02 ± 2.69	
$\log([\text{O III}]\lambda 5007/\text{H}\beta)$	0.07 ± 0.91	
$\log([\text{N II}]\lambda 6584/\text{H}\alpha)$	-0.45 ± 0.32	
$\log([\text{S II}]\lambda\lambda 6717, 6731/\text{H}\alpha)$	-0.19 ± 0.22	

fluxes $I(\lambda)$ (see Table 2) relative to $\text{H}\beta$ using the formula:

$$\frac{I(\lambda)}{I(\text{H}\beta)} = \frac{F(\lambda)}{F(\text{H}\beta)} \times 10^{c(\text{H}\beta)f(\lambda)}$$

where $f(\lambda)$ is the reddening function given by CCM assuming $R_V = 3.1$, $c(\text{H}\beta)$ is logarithmic reddening parameter calculated for case B, assuming Balmer decrement ratio $\text{H}\alpha/\text{H}\beta = 2.86$ at 10,000 K, from Osterbrock & Ferland (2006).

The $12 + \log(\text{O}/\text{H})$ mean of all the Table 1 calibrators was 8.68 with a standard deviation of 0.14 dex. Compared to other dwarf galaxies in the literature (e.g., Lee et al. 2003), our $12 + \log(\text{O}/\text{H})$ value is high and approximately solar ($12 + \log(\text{O}/\text{H}) = 8.69$; Asplund et al. 2009), within the uncertainties, and is comparable to that of TDGs in the literature (see Figure 1). We summarize the properties of J2306 in Table 3.

2.2. GMRT H I Observations of J2306

J2306 was observed in H I at 21 cm using the GMRT on 2022 May 30th, with the pointing center at the projected position of J2306. A 12.5 MHz bandwidth was used giving a channel resolution ~ 6 kHz. The observation details are listed in Table 4. The H I data was analyzed using standard reduction procedures with the Astronomical Image Processing System (AIPS) software package. The flux density scale used was from Baars et al. (1977) with uncertainties of $\sim 5\%$. After bad data due to RFI and faulty antennas were flagged, the data was calibrated and continuum subtracted in the uv-domain. The AIPS task IMAGR was then used to convert the uv-domain data to three-dimensional H I image cubes. To study the H I distribution in detail, image cubes with different spatial resolutions were made by varying the uv limits and applying different “tapers” to the data. Finally, the AIPS task MOMNT was used to create the integrated H I images and the velocity field maps from the H I image cubes. Properties of the low and medium-resolution maps presented in this paper are given in Table 4.

Table 3
Properties of J2306

Property	Value	Unit
Redshift	0.005	
Distance	22.7	Mpc
g band magnitude	-14.83	mag
$g - r$	0.23^a	mag
$12 + \log(\text{O}/\text{H})$	8.68	
D_{25}	2.9	kpc
Stellar mass	2.4×10^7	M_\odot
H I mass	4.3×10^8	M_\odot
Dynamical mass	6.4×10^9	M_\odot

Note.

^a The galaxy has an SDSS unreliable flag on its photometry. The error on the color is ~ 0.12 . Therefore we treat the stellar mass, estimated using this color, as an order of magnitude estimate.

Table 4
GMRT Observational and H I Map Parameters

Rest frequency	1420.4057 MHz
Observation Date	2022 May 30th
Integration time	9.0 hr
Primary beam	24' at 1420.4057 MHz
Low-resolution (beam-FWHP)	$38''.9 \times 36''.9$, PA = -18°
Medium-resolution beam-FWHP	$24''.5 \times 21''.5$, PA = $9^\circ 5'$
rms per channel for low-resolution map	$3.0 \text{ mJy beam}^{-1}$
rms per channel for medium-resolution map	$2.9 \text{ mJy beam}^{-1}$
R.A. (pointing center)	$23^{\text{h}}06^{\text{m}}15^{\text{s}}.0$
decl. (pointing center)	$14^\circ 39' 27''.6$

3. Results

The low-resolution GMRT integrated H I and velocity field images reveal J2306's H I disk to be extended and to a first order unperturbed. The left panel of Figure 4 shows the low-resolution ($38''.9 \times 36''.9$) velocity integrated H I flux density contours and the right panel shows the H I velocity field for J2306, respectively. Figure 5 shows the medium-resolution ($24''.5 \times 21''.5$) velocity integrated H I flux density contours for the galaxy. At the distance of the galaxy, 22.7 Mpc, the $38''.9$ and $24''.5$ GMRT beams sample 4.3 and 2.7 kpc, respectively. While the low-resolution H I disk morphology appears highly symmetric and undisturbed, the medium-resolution image shows the highest column density H I has a more irregular structure, with an overall alignment along an NW to SE axis. This is not unexpected, given that J2306 is a dwarf galaxy, and dwarfs are well known to have irregular H I density distributions. The medium-resolution H I column density maximum spatially coincides with the optical galaxy.

The low-resolution H I velocity field shows a regularly rotating disk. The velocity field maps are intensity weighted, and we present the low-resolution map here since it has a higher

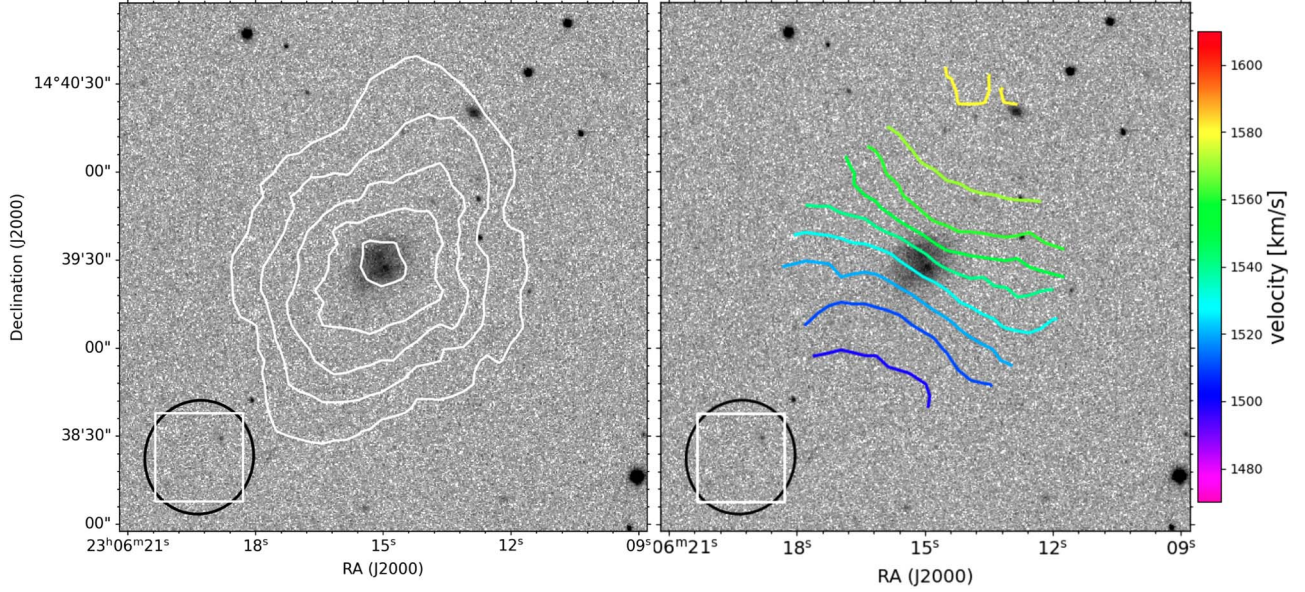


Figure 4. J2306 low-resolution ($38''9 \times 36''9$) GMRT moment maps. Left: velocity integrated total H I map overlaid on SDSS *g*-band image. The H I column density contour levels are $10^{19} \text{ atoms cm}^{-2} \times (6.7, 15.7, 27.7, 33.7, 47.1)$. Right: velocity field of the galaxy overlaid on a SDSS *g*-band image. The contours are from 1500 to 1580 km s^{-1} , inclusive, in steps of 10 km s^{-1} , per the color scale. The synthesised beam is plotted using a black ellipse at the bottom left of both the images. The white box on the ellipse denotes $30' \times 30'$ area.

signal-to-noise ratio. The regular rotation of the H I disk is consistent with the single dish Arecibo spectrum's double horn profile which suggests a rotating H I disk. Resolved H I imaging of the galaxy reveals the absence of any neighbor or companion galaxy within the GMRT $24'$ primary beam, confirming the entire H I mass detected with Arecibo belongs to J2306.

A comparison between the Arecibo and GMRT spectra of the galaxy confirms most of the H I flux was recovered in the GMRT interferometric imaging. Usually for extended objects, flux loss occurs in the interferometric data due to a combination of several factors, namely flagging of crucial short baselines due to RFI, flagging of bad data leading to insufficient uv coverage and resolving out of the extended emission. Hence when available, it is preferable to carry out the global H I estimates, such as H I mass, using the single dish spectrum data. Of course to use the single dish H I flux to estimate a galaxy's H I mass it is necessary to ensure that there is no contamination from other sources within the single dish full width half power (FWHP) beam. In J2306's case the GMRT data allows us to confirm that there are no contaminating H I sources within the single dish beam. Using the integrated flux density from the Arecibo spectrum ($3.54 \text{ Jy km s}^{-1}$), we estimate the H I mass of J2306 using Equation (2):

$$M(\text{H I}) = 2.36 \times 10^5 \times D^2 \times \int S_\nu dv \quad (2)$$

Here, D is the distance to J2306 (22.7 Mpc) and $\int S_\nu dv$ is the integrated flux density from the Arecibo spectrum. The H I

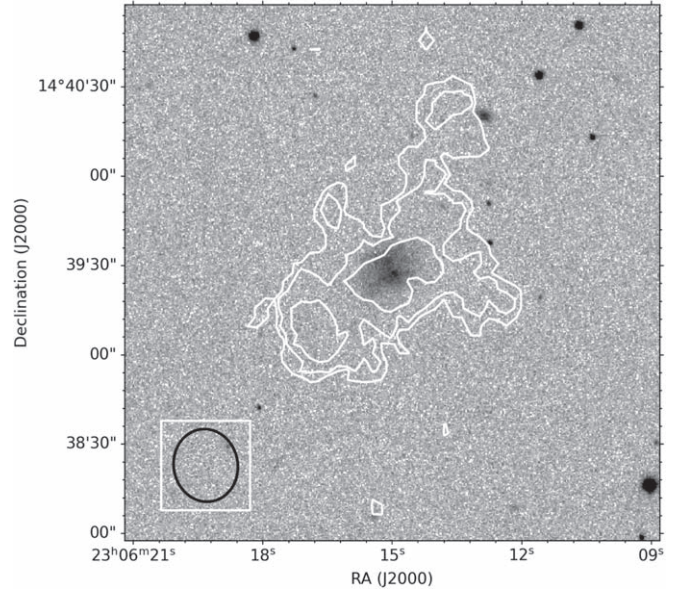


Figure 5. J2306 medium-resolution ($24''5 \times 21''5$) velocity integrated H I map overlaid on SDSS *g*-band image of the galaxy. The H I column density contour levels are $10^{19} \text{ atoms cm}^{-2} \times (5.2, 8.6, 17.3)$. The synthesised beam is plotted using a black ellipse at the bottom left of the image. The white box on the ellipse denotes $30' \times 30'$ area.

mass of J2306, thus calculated is $\sim 4.3 \times 10^8 M_\odot$. This implies the galaxy's $M_{\text{HI}}/M_* \sim 18$. Even taking into account the caveat about the galaxy's stellar mass in Section 2.1 these ratios

indicate that J2306 is an H I rich dwarf galaxy. Here M_* and D_{25} were estimated from the SDSS photometric data and NED respectively and their values were used in compiling Table 3.

4. Discussion

Since the dwarf galaxy population is dominated by low metallicity objects (e.g., Kunth & Östlin 2000; Lee et al. 2003), the rarely found high-metallicity dwarfs are of particular interest (Peeples et al. 2008). One pathway to a high-metallicity dwarf is a result of tidal interactions between larger gas rich galaxies. During tidal interactions between such galaxies, gas rich tidal debris can form TDGs ($M_* \sim 10^7\text{--}10^8 M_\odot$). The collapsing metal-rich gas debris is predicted to lead to rotating H I and molecular disks and in turn in-situ star formation (SF) in the TDGs. Being born of tidal debris, TDGs are expected to have significantly higher metallicities and little or no DM content compared to normal dwarfs (Duc & Mirabel 1999; Boquien et al. 2010; Duc et al. 2014). Another possible pathway to high-metallicity dwarf could be the accretion of nearby high-metallicity companions. Given the small size of J2306, any recently accreted companion would have been an even smaller metal-rich dwarf galaxy. Here we discuss the environment of J2306, estimate its dynamical mass and explore possible scenarios under which it could have attained such high metal abundances.

To understand the environment of J2306, we searched for neighboring galaxies using the NED database. At J2306's distance, $60'$ is ~ 380 kpc. Thus a $60'$ radius search, with an optical velocity (V_{opt}) constraint of $200 \text{ km s}^{-1} \leq V_{\text{opt}} \leq 3500 \text{ km s}^{-1}$ was carried out using the NED database to search for neighboring galaxies. This search returned only three neighbors. One of them is HIPASS J2306+14, which is the HIPASS H I detection for J2306. There is a $\sim 4'$ difference between the HIPASS and WISE detected positions. However, the velocities and the HIPASS spectrum reveal them to be the same galaxy. The other two neighbors are AGES J230511+140404 and SDSS J230511.15+140345.7 at a projected distance of ~ 250 kpc from J2306. These two detections are at same redshifts and separated by less than 0.5 and are almost certainly detections of the same galaxy, with the magnitude of positional offsets within the large positional uncertainties of the Arecibo Galaxy Environment Survey (AGES) survey FWHP beam ($3/5$ Arecibo beam). It is difficult to identify and confirm isolated galaxies. The standard isolation criteria require no companions within a projected sky diameter of ~ 1 Mpc (Verley et al. 2007b). In that respect, J2306 can be considered a fairly isolated galaxy with only one galaxy within a projected diameter ~ 500 kpc and a velocity range of $200\text{--}3500 \text{ km s}^{-1}$. The relative isolation and the absence of obvious parent galaxy pair to generate the tidal debris from which to form a TDG makes the recent TDG formation scenario for J2306 highly unlikely.

This raises the interesting question of how, as an almost isolated dwarf galaxy, J2306 came to have a higher than average metallicity. SDSS J230511.15+140345.7 is the only galaxy with known redshift, within a diameter of 500 kpc of J2306. We studied its properties to see if this galaxy could have any effect on J2306's evolution. The galaxy is also a small dwarf galaxy, with an r -band $D_{25} \sim 0.3$ kpc (extracted from NED), $g-r$ color ~ 0.25 . This galaxy was detected in the AGES and it is H I mass according to AGES survey data is $1.2 \times 10^8 M_\odot$ (Davies et al. 2011). The optical size and the H I mass indicates that SDSS J230511.15+140345.7 is also a dwarf galaxy. SDSS J230511.15+140345.7 is separated from J2306 by a projected distance of 250 kpc. We estimated the timescale of a hypothetical past interaction between SDSS J230511.15+140345.7 and J2306. Considering their current positions, if both the galaxies moved apart at $\sim 200 \text{ km s}^{-1}$ (an average group dispersion velocity), the minimum distance covered by each of them would be 125 kpc. Since 250 kpc is their current projected separation, this suggests any past interaction would have taken place at least 6.3×10^8 yr ago. Such an interaction could in principle have increased the star formation and thereby enriched the gas in J2306. However, this timescale is too long for detectable signatures of interaction to remain identifiable in the H I disk of J2306, and thus we cannot draw any conclusion about this possibility. Even for massive spiral galaxies, signs of past perturbations or mergers are identifiable in their disks only for about $4\text{--}7 \times 10^8$ yr (Holwerda et al. 2011). Interestingly, this timescale is sufficient to enrich the ISM of J2306. Under such an interaction scenario the newly produced metals would be dispersed and mixed on $\sim 1\text{--}2$ kpc scales in around 10^8 yr (e.g., Tenorio-Tagle 1996; Lagos et al. 2009, 2016). One however cannot rule out the possibility of minor interactions or mergers of even lower mass metal-rich, early-type dwarfs surrounding J2306. More detailed spectroscopic data for J2306 might provide an answer about the feasibility of this option.

As discussed before, there are two well accepted criteria to identify a tidal dwarf galaxy, i.e., their higher than average metal abundance and their lack of DM. J2306 is a high-metallicity dwarf with an H I disk showing signs of regular rotation. We did not find any obvious progenitor galaxy pair near the dwarf galaxy. However, that cannot rule out that it is an old detached TDG which may have drifted away from its parent galaxy pair. We, therefore, estimated its dynamical mass to see if the galaxy is DM dominated or show signs of DM deficiency, within the measured H I radius. The ALFALFA Arecibo database shows the H I line width (W_{20}) to be $\sim 106 \text{ km s}^{-1}$. From the low-resolution GMRT H I map we estimated the approximate H I diameter of J2306 to be ~ 13.2 kpc and the inclination to be $\sim 54^\circ$. Using the inclination and the W_{20} value we estimated the inclination corrected rotation velocity (V_{rot}) $\sim 63 \text{ km s}^{-1}$ and the dynamical mass (M_{dyn}) of the galaxy to be

$\sim 6.4 \times 10^9 M_\odot$. Comparing the M_{dyn} to the baryonic mass

$$\frac{M_{\text{dyn}}}{M_{\text{gas}} + M_*} = 9.4,$$

where $M_* = 2.4 \times 10^7 M_\odot$, $M_{\text{gas}} = 65.2 \times 10^7 M_\odot$, i.e., M_{gas} (molecular + atomic) = $1.4 \times M_{\text{HI}}$ ($43.0 \times 10^7 M_\odot$). Even allowing for the uncertainty in our estimated stellar mass, this ratio implies, like most regular dwarf galaxies, the galaxy is strongly DM dominated within its H I radius. For TDGs this ratio would typically be closer to 1 (Sengupta et al. 2014, 2017). This reinforces our previous conclusion, based on its environment, that J2306 is almost certainly not a tidal dwarf galaxy.

To summarize, we explored some possible reasons that could account for J2306's high gas metallicity. High-metallicity is a signature of TDGs so we checked for signs that J2306 is a TDG. The lack of a nearby progenitor pair and the dominance of DM within the H I radius rule out the galaxy as a TDG. Additionally, we did not find any signs of recent accretion or merger that could be an alternative explanation for the high gas phase metallicity.

5. Conclusion



We studied the high-metallicity dwarf galaxy J2306 to investigate whether the galaxy could be a possible TDG candidate. The galaxy is not an early type dwarf, its $g - r$ color is 0.23 mag and its optical morphology is non-compact and irregular. GMRT H I mapping of the galaxy confirmed it was H I rich and its unperturbed and rotating disk extends ~ 4 times further than the optical disk. We found no signs of past or ongoing interactions in the H I images. Neither did we find any possible neighboring galaxy pair which could potentially be the parent system if J2306 was to be a TDG. Using information from the H I images, we estimated the dynamical mass of the galaxy. Contrary to what is expected for TDGs, J2306 was found to be a DM dominated galaxy. We explored other possibilities (e.g., interactions or accretions) for the origin of the high-metallicity of J2306. However, we found J2306 to be fairly isolated with only one neighboring galaxy within a projected diameter of 500 kpc. We conclude that while J2306 is a high-metallicity galaxy this property is neither of recent tidal origin, nor does it show any obvious signs of recent accretion or merger. It is located in a fairly isolated environment and thus its enrichment process could be a secular process, or the result of an interaction in the distant past. Further detailed spectroscopic observations of J2306 could provide an answer to how normal irregular dwarf galaxies can achieve such a level of metal enrichment.

Acknowledgments

We thank the staff of the GMRT who have made these observations possible. The GMRT is operated by the National

Centre for Radio Astrophysics of the Tata Institute of Fundamental Research. Y.G. acknowledges support from the National Key Research and Development Program of China (2022SKA0130100), and the National Natural Science Foundation of China (grant No. 12041306). P.L. (contract DL57/2016/CP1364/CT0010) and T.S. (contract DL57/2016/CP1364/CT0009) are supported by national funds through Fundação para a Ciência e a Tecnologia (FCT) and the Centro de Astrofísica da Universidade do Porto (CAUP). This research made use of APLpy, an open-source plotting package for Python (Robitaille & Bressert 2012). This research has made use of the Sloan Digital Sky Survey (SDSS). The SDSS Web Site is <http://www.sdss.org/>. This research has made use of the NASA/IPAC Extragalactic Database (NED) which is operated by the Jet Propulsion Laboratory, California Institute of Technology, under contract with the National Aeronautics and Space Administration.

ORCID iDs

Yan Guo  <https://orcid.org/0000-0002-9550-1937>
C. Sengupta  <https://orcid.org/0000-0002-7432-5225>
T. C. Scott  <https://orcid.org/0000-0002-3746-4859>
P. Lagos  <https://orcid.org/0000-0002-2321-8657>
Y. Luo  <https://orcid.org/0000-0003-2341-9755>

References

- Asplund, M., Grevesse, N., Sauval, A. J., & Scott, P. 2009, *ARA&A*, **47**, 481
- Baars, J. W. M., Genzel, R., Pauliny-Toth, I. I. K., & Witzel, A. 1977, *A&A*, **61**, 99
- Bell, E. F., McIntosh, D. H., Katz, N., & Weinberg, M. D. 2003, *ApJS*, **149**, 289
- Bian, F., Kewley, L. J., & Dopita, M. A. 2018, *ApJ*, **859**, 175
- Boquien, M., Duc, P. A., Galliano, F., et al. 2010, *AJ*, **140**, 2124
- Cardelli, J. A., Clayton, G. C., & Mathis, J. S. 1989, *ApJ*, **345**, 245
- Curti, M., Mannucci, F., Cresci, G., & Maiolino, R. 2020, *MNRAS*, **491**, 944
- Dale, D. A., Cohen, S. A., Johnson, L. C., et al. 2009, *ApJ*, **703**, 517
- Davies, J. I., Auld, R., Burns, L., et al. 2011, *MNRAS*, **415**, 1883
- Denicoló, G., Terlevich, R., & Terlevich, E. 2002, *MNRAS*, **330**, 69
- Duc, P.-A., & Mirabel, I. F. 1999, in *IAU Symp. 186, Galaxy Interactions at Low and High Redshift*, ed. J. E. Barnes & D. B. Sanders (Berlin: Springer), 61
- Duc, P.-A. 2012, in *Dwarf Galaxies: Keys to Galaxy Formation and Evolution* (Berlin: Springer), 305
- Duc, P.-A., Paudel, S., McDermid, R. M., et al. 2014, *MNRAS*, **440**, 1458
- Gomes, J. M., & Papaderos, P. 2017, *A&A*, **603**, A63
- Haynes, M. P., Giovanelli, R., Martin, A. M., et al. 2011, *AJ*, **142**, 170
- Holwerda, B. W., Pirzkal, N., Cox, T. J., et al. 2011, *MNRAS*, **416**, 2426
- Kunth, D., & Östlin, G. 2000, *A&ARv*, **10**, 1
- Lagos, P., Demarco, R., Papaderos, P., et al. 2016, *MNRAS*, **456**, 1549
- Lagos, P., Scott, T. C., Nigoche-Netro, A., et al. 2018, *MNRAS*, **477**, 392
- Lagos, P., Telles, E., & Melnick, J. 2007, *A&A*, **476**, 89
- Lagos, P., Telles, E., Muñoz-Tuñón, C., et al. 2009, *AJ*, **137**, 5068
- Lee, H., Grebel, E. K., & Hodge, P. W. 2003, *A&A*, **401**, 141
- Marino, R. A., Rosales-Ortega, F. F., Sánchez, S. F., et al. 2013, *A&A*, **559**, A114
- McConnachie, A. W. 2012, *AJ*, **144**, 4
- Nagao, T., Maiolino, R., & Marconi, A. 2006, *A&A*, **459**, 85
- Oh, S.-H., Hunter, D. A., Brinks, E., et al. 2015, *AJ*, **149**, 180
- Osterbrock, D. E., & Ferland, G. J. 2006, *Astrophysics of Gaseous Nebulae and Active Galactic Nuclei* (2nd ed.; Sausalito, CA: Univ. Science Books)

- Peebles, M. S., Pogge, R. W., & Stanek, K. Z. 2008, [ApJ](#), **685**, 904
- Pérez-Montero, E., & Contini, T. 2009, [MNRAS](#), **398**, 949
- Pettini, M., & Pagel, B. E. J. 2004, [MNRAS](#), **348**, L59
- Planck Collaboration, Aghanim, N., Akrami, Y., et al. 2020, [A&A](#), **641**, A6
- Richer, M. G., & McCall, M. L. 1995, [ApJ](#), **445**, 642
- Robitaille, T., & Bressert, E., 2012 APLpy: Astronomical Plotting Library in Python, Astrophysics Source Code Library, ascl:[1208.017](#)
- Schlegel, D. J., Finkbeiner, D. P., & Davis, M. 1998, [ApJ](#), **500**, 525
- Scott, T. C., Lagos, P., Ramya, S., et al. 2018, [MNRAS](#), **475**, 1148
- Sengupta, C., Scott, T. C., Dwarakanath, K. S., Saikia, D. J., & Sohn, B. W. 2014, [MNRAS](#), **444**, 558
- Sengupta, C., Scott, T. C., Paudel, S., et al. 2017, [MNRAS](#), **469**, 3629
- Smith, B. J., Giroux, M. L., Struck, C., & Hancock, M. 2010, [AJ](#), **139**, 1212
- Tenorio-Tagle, G. 1996, [AJ](#), **111**, 1641
- Tremonti, C. A., Heckman, T. M., Kauffmann, G., et al. 2004, [ApJ](#), **613**, 898
- van Zee, L., & Haynes, M. P. 2006, [ApJ](#), **636**, 214
- Verley, S., Leon, S., Verdes-Montenegro, L., et al. 2007b, [A&A](#), **472**, 121
- Weilbacher, P. M., Duc, P. A., & Fritze-v. Alvensleben, U. 2003, [A&A](#), **397**, 545